

Targeting Human Central Nervous System Protein Kinases: An Isoform Selective p38 α MAPK Inhibitor That Attenuates Disease Progression in Alzheimer's Disease Mouse Models

Saktimayee M. Roy,[†] Valerie L. Grum-Tokars,[†] James P. Schavocky,[†] Faisal Saeed,[‡] Agnieszka Staniszewski,[‡] Andrew F. Teich,[‡] Ottavio Arancio,[‡] Adam D. Bachstetter,[§] Scott J. Webster,[§] Linda J. Van Eldik,[§] George Minasov,[†] Wayne F. Anderson,[†] Jeffrey C. Pelletier,[†] and D. Martin Watterson^{*,†}

[†]Northwestern University, Chicago, Illinois 60611, United States

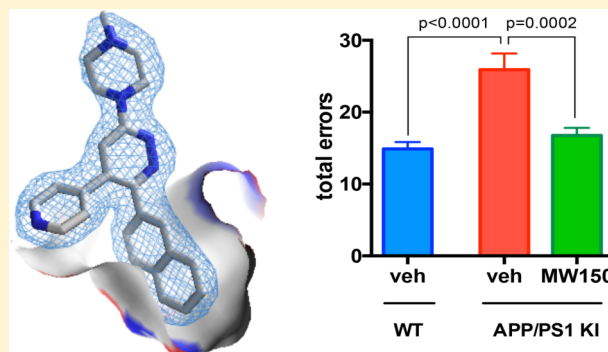
[‡]Columbia University, New York, New York 10032, United States

[§]University of Kentucky, Lexington, Kentucky 40536, United States

S Supporting Information

ABSTRACT: The first kinase inhibitor drug approval in 2001 initiated a remarkable decade of tyrosine kinase inhibitor drugs for oncology indications, but a void exists for serine/threonine protein kinase inhibitor drugs and central nervous system indications. Stress kinases are of special interest in neurological and neuropsychiatric disorders due to their involvement in synaptic dysfunction and complex disease susceptibility. Clinical and preclinical evidence implicates the stress related kinase p38 α MAPK as a potential neurotherapeutic target, but isoform selective p38 α MAPK inhibitor candidates are lacking and the mixed kinase inhibitor drugs that are promising in peripheral tissue disease indications have limitations for neurologic indications. Therefore, pursuit of the neurotherapeutic hypothesis requires kinase isoform selective inhibitors with appropriate neuropharmacology features. Synaptic dysfunction disorders offer a potential for enhanced pharmacological efficacy due to stress-induced activation of p38 α MAPK in both neurons and glia, the interacting cellular components of the synaptic pathophysiological axis, to be modulated. We report a novel isoform selective p38 α MAPK inhibitor, MW01-18-150SRM (=MW150), that is efficacious in suppression of hippocampal-dependent associative and spatial memory deficits in two distinct synaptic dysfunction mouse models. A synthetic scheme for biocompatible product and positive outcomes from pharmacological screens are presented. The high-resolution crystallographic structure of the p38 α MAPK/MW150 complex documents active site binding, reveals a potential low energy conformation of the bound inhibitor, and suggests a structural explanation for MW150's exquisite target selectivity. As far as we are aware, MW150 is without precedent as an isoform selective p38MAPK inhibitor or as a kinase inhibitor capable of modulating in vivo stress related behavior.

KEYWORDS: Signal transduction, cognitive dysfunction, protein kinase, crystallography, chemical synthesis, pharmacology



The approval of Gleevec in 2001 provided the first kinase inhibitor drug.¹ Gleevec is a multikinase inhibitor that binds at the active site of tyrosine kinases.^{2,3} Subsequent approved kinase inhibitor drugs shared the features of active site binding and multikinase targeting.²⁻⁴ These early historical development trends contributed to prevailing bias and perspectives.²⁻⁴ For example, one concern was that in vivo function might require drug candidates to have multikinase activity.² Another concern was that development of kinase inhibitor drugs would be limited if one targeted the active site, due to the level of sequence similarity of catalytic domains across the kinome family and the high levels of ATP in the eukaryotic cell.^{2,4,5} However, the kinase active site continues to

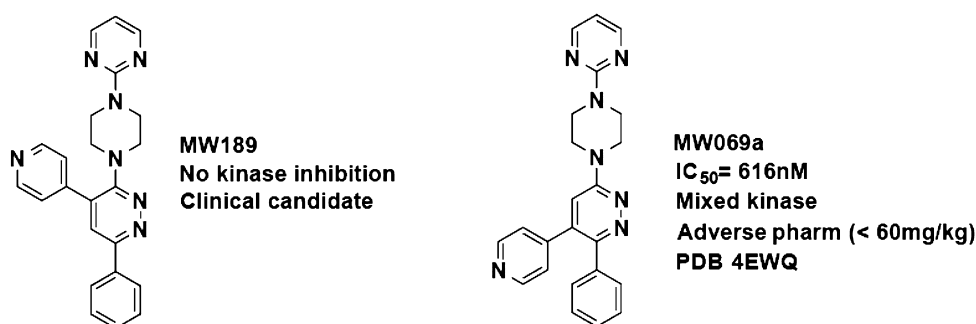
be highly druggable as documented by the approved kinase inhibitor drugs that target the active site.³ In addition, progress in recent years indicates the feasibility of generating new kinase inhibitor drug candidates with even greater selectivity through medicinal chemistry optimization driven by structural biology approaches.^{2,6} Regardless, the above concerns and the estimate that only about 2% of small molecule drugs have adequate blood brain barrier distribution⁷ have led to the perspective that

Received: January 3, 2015

Revised: February 11, 2015

Published: February 13, 2015

Scaffold Repurposing Using Target Crystallography & Pharmacology Filter



SAR: Decrease Adverse Pharmacology, Generate Isoform Specificity & Improve Bioavailability Potential

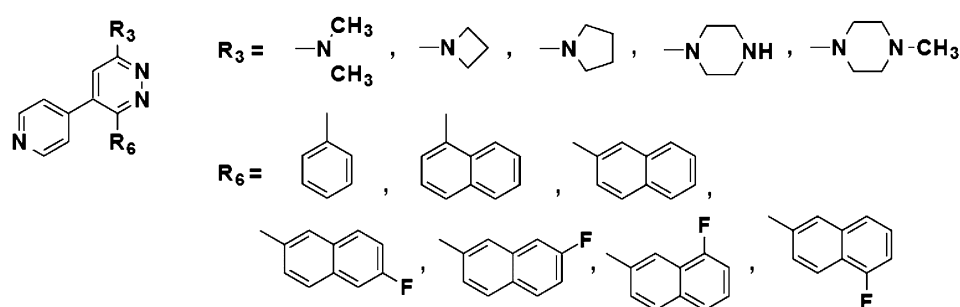


Figure 1. Repurposing of a nonkinase CNS experimental therapeutic to CNS kinase inhibitor.

kinases are not a promising class of central nervous system (CNS) drug development targets.

Clearly, major gaps remain in the protein kinase inhibitor drug pipeline,^{3–6} including: (1) the limited number of validated protein kinase targets outside oncology indications; (2) the paucity of serine/threonine (S/T) protein kinase inhibitor drugs; and (3) the absence of approved CNS kinase inhibitor drugs. Successful targeting of CNS S/T kinases represents an intertwined triple challenge. First, there is the inherent tissue barrier challenge of CNS drug development.⁷ Second, there is an insufficient number of single kinase-specific *in vivo* small molecule tools for target validation studies.^{3,5,6} Initial target validation requires evidence for modulation by selective probes. While genetic knock down and chemical proteomics studies are key for discovery, inherent limitations of the latter approaches, including the potential of an observed phenotype being indirect due to an effect on the kinase interactome, do not allow them to stand alone for initial target validation.^{5,10,11} The ideal is to complement the broader discovery approaches with direct *in vivo* molecular probe approach, but this can be technically challenging. Third, intracellular S/T kinases are nodes in an integrated system¹¹ in which the *in vivo* function of a widely distributed enzyme is dependent on the context of tissue physiological state as well as molecular partners and cellular localization. Because alteration of phenotype does not require full activation of all kinase nodes in the network, it is not currently possible to forecast what percentage inhibition of the fractionally activated network will result in restoration of homeostasis. It is critical, therefore, that individual CNS S/T protein kinases be examined for their potential pharmacological modulation with selective *in vivo* probes and that CNS drug candidates with these attributes be developed.^{3,6,8,10}

A potential neurotherapeutic kinase target identified across diverse disease areas is p38 α MAPK, a S/T protein kinase implicated in various stress-induced activations within neurons and glia, the cellular components of the synaptic physiologic axis that manifests dysfunction across multiple dementia and neurodegenerative disorders.^{6,8,10,12–23} However, deconvolution of p38 α MAPK's exact signaling function for a given *in vivo* physiological or pathophysiological role is complicated by a number of factors,^{6–10} including: (1) wide tissue distribution; (2) presence as a mixture of phosphorylated and non-phosphorylated states that differ in activity; (3) protein–protein interactions that control subcellular localizations; and (4) the presence of parallel interactive signaling pathways responding to the same cellular stressors as part of an integrated system-wide network. Regardless of the mechanistic knowledge gaps, recent evidence from *in vivo* studies with selective p38 α MAPK inhibitor molecular probes⁶ demonstrated attenuation of neuroinflammation, synaptic dysfunction, and cognitive deficits, thereby providing a more direct pharmacological link among mechanism of action, pharmacodynamics, and efficacy. However, issues of metabolic stability, CYP substrate status, and oral bioavailability limit the potential use of these *in vivo* probes for drug development in complex diseases that require extended exposure, repeat administration, and low potential for drug–drug interactions via CYP substrate or inhibitor status.

The accumulating body of evidence for CNS p38 α MAPK as a target offers the potential of an unusual pharmacological strategy where the same inhibitor might be used to attenuate stressor induced pathophysiological responses in two interacting cells, glia and neurons, within the synaptic structure. Targeting such a localized neuropathophysiology axis could

offer an enhanced potential for efficacy.^{3,6} For example, an enhanced potential for efficacy could arise if both the endogenous glia and neuron pathways are key to pathophysiology progression during a common intervention time window. In addition, a potential for an extended efficacy time window might occur if the importance of activated glia is key early in progression and neuronal stress is more critical at later time windows of progression, allowing for the same drug to have extended pharmacodynamics via action in overlapping but distinct pathology progression time windows. Dosing, the pharmacological basis of therapeutics, would allow the probing of such possibilities once a candidate therapeutic is obtained. However, the future testing of various neurotherapeutic hypotheses involving p38 α MAPK requires a priori the availability of a highly selective p38 α MAPK inhibitor candidate with appropriate pharmacological properties.

As a further step toward addressing the hypothesis of p38 α MAPK as a potential neurotherapeutic target, we report here the synthesis and functional characterization of MW01-18-150SRM (referred to as MW150), a novel selective inhibitor of the p38 α MAPK isoform with promising pharmacological features and in vivo CNS efficacy. Memory loss is the clinical hallmark of Alzheimer's disease (AD), and drugs approved for AD employ the attenuation of memory loss as a qualifying end point. Therefore, we used a detailed behavioral assessment of memory as the initial relevant pharmacodynamic readout for MW150 efficacy. Two independent mouse models of AD relevant pathophysiology progression were employed. One is a transgenic model with rapid pathophysiology progression. The other is a humanized knock-in model that employs endogenous promoters and exhibits age-related pathophysiology progression over an extended time frame. The in vivo efficacy of MW150 is consistent with a true hippocampus-dependent mechanism of action in attenuation of memory deficits. Key pharmacological screens of MW150 indicate the potential for compatible use with approved AD drugs. In aggregate, the results are consistent with future pursuit of MW150 as a logical drug candidate. Molecular level characterization of MW150 by high resolution crystallography of the human p38 α MAPK/MW150 complex documents MW150's active site occupancy with key intermolecular interactions, indicates that the active site bound inhibitor is in a relative low energy conformation, and provides a rational explanation for the molecular basis of MW150 exquisite selectivity. Overall, the results are consistent with MW150 being a unique candidate for the in vivo study of CNS function and dysfunction, provide a precedent for kinase active site targeting to attain highly selective kinase inhibitors with in vivo CNS function, and support the concept of attenuating behavioral deficits through the use of protein kinase inhibitors.

RESULTS AND DISCUSSION

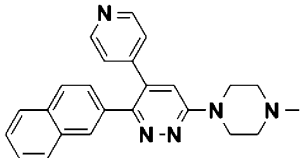
Rationale and Overview. The scaffold repurposing approach^{6,12} that delivered MW150 employed high-resolution crystallography of complexes containing human p38 α MAPK combined with small molecule design using pharmacoinformatics considerations. Synthesized inhibitors were curated by activity and pharmacological screening.^{6,12} The initial hit, MW069a,¹² was obtained by alternative placement of the pyridine substituent on the pyridazine core of a safe, brain penetrant experimental therapeutic, MW189²⁴ (Figure 1). MW189 attenuates neurotoxic overproduction of cytokines by activated glia back toward normal, has no reported direct

therapeutic effects on neurons, and is negative in kinome-wide screens. The alternative placement of the pyridine ring to produce MW069a generated a key H-bonding interaction with the p38 α MAPK hinge region backbone and allowed occupancy by the phenyl substituent of the nearby hydrophobic pocket (see PDB entry 4EWQ). MW069a lacks inhibitor activity with p38 α MAPK(T106M), the enzymatically active point mutant in which the introduction of a bulky amino acid at the entrance to the hydrophobic pocket prohibits access by ligand aromatic substituents, provided a link between crystal structure of the complex and in vitro inhibition activity.¹² Although MW069a has in vivo function in an Alzheimer's disease relevant screening assay,¹² it is a mixed kinase inhibitor like extant p38 α MAPK inhibitor drugs and has a limited safety with dose escalation. Therefore, pharmacological safety was improved next⁶ by reduction in the size of the exocyclic amine substituent. The p38 α MAPK specificity and affinity was also improved⁶ through the introduction of a 2-naphthyl substituent at the R₆ position (Figure 1). The simplest of the resultant naphthylpyridazinylpyridines (MW181, PDB 4F9Y; MW108, PDB 4F9W) retain the key target interactions, engage in a dose dependent manner the endogenous p38 α MAPK in activated glia, and are selective as demonstrated by kinome-wide activity screens and inactivity with the p38 α MAPK(T106M) drug resistant knock-in mouse glia.⁶ However, further exploration of in vivo function and the potential for preclinical drug development was limited by their potential for metabolism and distribution as evidenced by human liver microsome (HLM) screening assay outcomes of $T_{1/2} = 18$ min (MW181) and $T_{1/2} = 33$ min (MW108).

As summarized herein, a final optimization by synthesis and screening yielded MW150 that has improved HLM stability ($T_{1/2} > 60$ min) and oral bioavailability (>50%) as well as an incrementally improved p38 α MAPK inhibition activity with retention of target selectivity, safety, and brain penetrance. A summary of key MW150 features described in the following sections is provided in Table 1. Attempts at further improvement in metabolic stability potential were addressed through synthesis and testing of R₃ amine analogues and R₆ fluoronaphthyl analogues of MW150 (Supporting Information Table S1) that did not yield significant improvement in multiproperty features. For example, fluoronaphthyl analogues did not improve HLM stability and, in some cases, resulted in loss of activity. MW150, containing a R₃ piperazine substituent and R₆ 2-naphthyl substituent, represents the best in class for metabolic and bioavailability potential with retention of isoform selective p38 α MAPK IC₅₀ activity. Overall, the results demonstrate that the active site of this protein kinase can be targeted to generate an isoform selective inhibitor with in vivo CNS efficacy. The molecular and pharmacological profile describes a unique deliverable appropriate for future investigational new drug (IND) enabling preclinical development.

Chemistry. MW150, 6-(4-methylpiperazin-1-yl)-3-(naphthalen-2-yl)-4-(pyridin-4-yl)pyridazine (8 = MW150), and its hydrochloride salt (9) were made via an eight step, multigram scale, synthetic scheme (Scheme 1) with a final product (purity, 96%) appropriate for biological investigations. The details and the characterization of intermediate and final products in Scheme 1 are provided in Methods. Briefly, 2-naphthoyl chloride was reacted with *N,O*-dimethylhydroxyl amine to provide the Weinreb amide 2 in quantitative yield. Treatment of 2 with the lithio salt of 4-picoline gave the expected ketone 3, which was further reacted with sodium hydride and ethyl bromoacetate to form the ketoester intermediate 4. Reaction of

Table 1. Summary Data Sheet for MW150

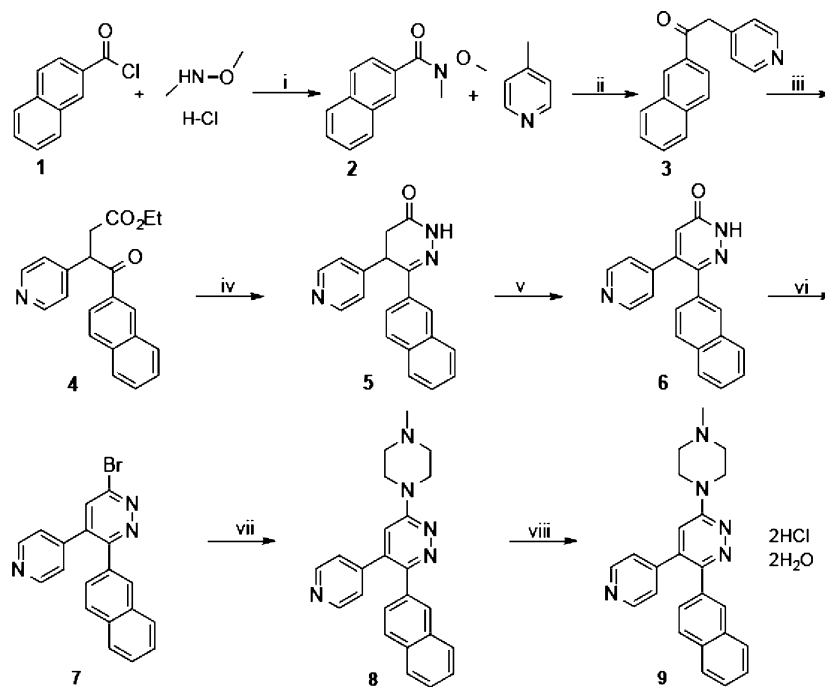


MW (base)	381.47
MW (hydrochloride hydrate)	490.43
cLogP	2.18
PSA	45.15
chemical stability	stable at pH (1–13), 24 h, 37 °C
solubility (hydrochloride hydrate)	>1 mg/mL
pK _a (potentiometric; spectrophotometric)	3.83, 7.27; 3.62, 7.27
apparent target affinity	K _i = 101 nM (p38αMAPK)
target cocystal structure	PDB 4R3C; 2 Å
kinome target class selectivity	negative except p38αMAPK
functional GPCR off-target activity	negative
Caco-2 permeability/P-gp substrate	highly permeable; not P-gp substrate
MDCK permeability/BCRP substrate	highly permeable; not BCRP substrate
human liver microsome stability	T _{1/2} > 60 min
human CYP substrate	negative: 1A2, 2B6, 2D6, 2C8, 2C9, 2C19, 3A4
human CYP inhibition	negative: 1A2, 2B6, 2D6, 2C8, 2C9, 2C19, 3A4
MAO-A/MAO-B inhibition	negative
AMES test	negative
oral Bioavailability	>50%
Brain/plasma ratio	>0.9

4 with hydrazine gave the expected dihydropyridazinone 5, which was oxidized to 6 with aqueous NBS in DMSO.

Conversion to the bromide 7 occurred following treatment with phosphorus oxybromide in acetonitrile. The free base of the final product 8 was obtained when bromide 7 was treated with 1-methylpiperazine. The crystalline substance was treated with HCl to give the final salt form 9. The final hydrochloride salt form (9) was confirmed by elemental analysis and has acceptable water solubility (>1 mg/mL) for use in the biological studies reported here. The attractiveness of the scheme combined with the atomic resolution crystal structure of the human protein target and the small molecule candidate (Figure 2; PDB 4R3C) also provides a platform for facile incorporation of any future optimizations that might be desired.

Structure. The crystal structure of the complex containing human p38αMAPK and MW150 (PDB 4R3C) is of high quality (Table 2 and Figure 2). As discussed recently,²⁹ the issue of ligand geometry accuracy and the evaluation of parameters involved in protein ligand contacts are critical to interpretation of crystallography results in terms of target recognition and the implications for mechanism. Further, widely used virtual screening approaches in drug discovery are critically dependent on the robustness of experimental database entries based on crystallography. The paucity of isoform selective kinase inhibitors or CNS penetrant kinase inhibitors with in vivo function make the robustness of data evaluation even more critical. Table 2 statistics demonstrate a good fit of the diffraction data and the structural model for p38αMAPK. Further, there is a good fit of the inhibitor MW150 diffraction data (Figure 2). The results are consistent with an energetically favorable conformation of the piperazine ring in the target bound form of the inhibitor. Overall, the quality of the

Scheme 1^a

^aReagents and conditions: (i) DIPEA, DCM: 100%; (ii) LDA, THF, −78 °C, 83%; (iii) 60% NaH, 1,4-dioxane, 20 °C, ethyl 2-bromoacetate, 1 h; (iv) N₂H₄ AcOH, ethanol, reflux, 20 h; (v) NBS, DMSO/H₂O, 72 h = 97%; (vi) POBr₃, ACN, reflux, 10 h, 60%; (vii) 1-methylpiperazine, EtOH, reflux = 18 h, 94%; (viii) 2.5 equiv conc HCl, anhydrous isopropanol, 80 °C, 96%.

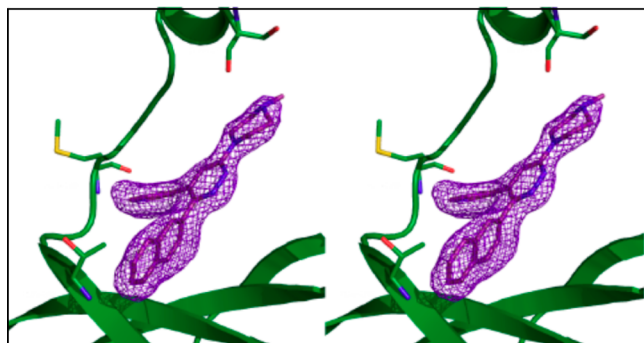


Figure 2. Stereo view of omit map for MW150 bound in the active site of human p38 α MAPK. The map represents the difference electron density (mesh) contoured at 2.5σ . The analysis indicates the goodness of fit between the model and experimental data and is consistent with an energetically favorable conformation for MW150 (purple). Key amino acids in p38 α MAPK (green) indicated: Met 109, involved in H-bonding with MW150, and Thr 106, gate-keeper for access to the hydrophobic pocket.

Table 2. Crystallographic Data and Refinement Statistics for the Human p38 α MAPK-MW150 Complex (PDB accession code 4R3C)

data collection	
space group	$P2_12_1$
wavelength (Å)	0.97872
cell dimensions	65.85, 74.51, 77.80, 90, 90, 90
resolution (Å)	30.00–2.05
outer resolution	2.09–2.05
completeness (%)	99.8 (100.0)
R_{merge}	0.062 (0.599)
mean (I/σ)	23.17 (2.37)
redundancy	4.8 (4.9)
no. of unique reflections	24 314
refinement	
resolution (Å)	29.93–2.06
R_{work}	17.5
R_{free}	21.6
RMSD bond lengths (Å)	0.009
RMSD bond angles (deg)	1.39

diffraction data and its fitting to the structural model provides increased confidence in evaluations of key interactions between human p38 α MAPK and MW150.

Inspection of the crystallographic structure reveals that MW150 and human p38 α MAPK retain the key complementary interactions that drove the discovery approach. Key conserved interactions within the active site (Figure 3A) include the hydrogen bond interaction between the pyridine ring nitrogen of MW150 and the amide backbone at Leu108-Met109 (Figure 3B) and occupancy of the proximal hydrophobic pocket by the naphthyl substituent of MW150 (Figure 3C). MW150 appears to use a single hydrogen bond interaction with the hinge region and does not induce significant localized conformational changes in the human p38 α MAPK active site. Notably, prior work showed that the crystallographic experimental approach is validated for the detection of such localized conformational changes in the hinge region should they be present.⁶ The significant space filling of the hydrophobic pocket by the naphthyl substituent is illustrated in the surface representation generated by residues within a 5 Å distance (Figure 3C). The

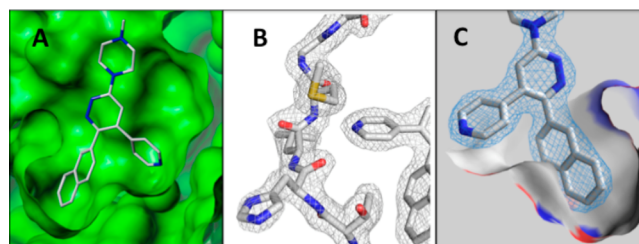


Figure 3. Human p38 α MAPK active site occupancy by MW150 (PDB 4R3C). (A) Connolly surface representation of the active site of p38 α MAPK containing MW150. (B) Close-up view of the p38 α MAPK hinge region near Met109 (left) and the pyridine substituent of MW150 (right) that are involved in hydrogen bond interaction. The gray mesh represents the experimental 2Fo-Fc electron density contoured at 1.2σ . (C) Surface created by amino acids within 5 Å of the naphthyl group of MW150. This perspective highlights the volume that the naphthyl substituent of MW150 occupies within the p38 α MAPK hydrophobic pocket that is proximal in space to the hydrogen-bonding region shown in panel (B). The blue mesh surrounding MW150 was built from the experimental 2Fo-Fc electron density contoured at 1.5σ .

greater space filling function of the naphthyl group, in the context of the other interactions such as the canonical hydrogen bonding with the hinge region, contributes to target affinity and selectivity. The structural results, combined with the large scale target screening data presented in the following section, suggest that the intimate pocket occupancy is a key contributor to specificity via the exclusion of MW150 binding to other targets in the proteome that either lack, or have less accommodating, proximal pockets. Overall, the most parsimonious model for this precedent of kinase isoform selectivity via targeting of the active site is one that maximizes of key chemical complementarities between MW150 and p38 α MAPK.

Kinome Target Selectivity. A large-scale hierarchical kinase screen approach⁶ was used to demonstrate (Table 3) the selectivity of MW150 for p38 α MAPK within the protein and lipid kinome. Briefly, 301 protein and lipid kinases representative of all major human kinome branches as well as isoforms of individual families were screened using substrates optimized for each kinase. The database accession numbers of the protein and lipid kinases shown in Table 3 are provided in Supporting Information Table S2. The only validated positive hit from the large scale kinome screen with an $IC_{50} < 1000$ nM was p38 α MAPK (Table 3). The estimated K_i from kinetic analyses (Supporting Information Figure S1) is 101 nM. Especially noteworthy (Table 3) is the failure of MW150 to inhibit significantly the other p38MAPK isoforms. The IC_{50} for p38 α MAPK inhibition is approximately 10-fold better than that for p38 β MAPK, 14-fold better than that for p38 δ MAPK, and 6-fold better than that for the atypical NLK. Further, MW150 does not inhibit the enzymatically normal p38 α MAPK-(T106M) point mutant in which the gatekeeper amino acid threonine is mutated to a bulkier methionine residue, thereby blocking access by the naphthyl substituent to the hydrophobic pocket. The kinome screening results are, therefore, consistent with the high resolution crystal structure of the complex.

The secondary assays for quantitative cellular activity of MW150 were done using a relevant CNS cell population, activated glia. As shown in Figure 4A, treatment of activated glia with MW150 inhibits in a concentration-dependent manner the ability of the endogenous p38 α MAPK to phosphorylate an endogenous substrate, MK2. These results

Table 3. Large Scale Hierarchical Kinome Screen

kinase ^a	H ^b	kinase ^a	H ^b	kinase ^a	H ^b	kinase ^a	H ^b	kinase ^a	H ^b	kinase ^a	H ^b	kinase ^a	H ^b	kinase ^a	H ^b
Abl	-	CDK5/p25	-	EGFR(790M)	-	GSK3 β	-	MARK1	H ^b	PAK5	-	PAK5	-	PKC η	-
Abl(396P)	-	CDK5/p35	-	EGFR(790M_858R)	-	Hasp1in	-	MELK	-	PAK6	-	PAK6	-	PKC μ	-
Abl(351T)	-	CDK6/eyD3	-	EphA1	-	Hck	-	Mer	-	PAR-1B α	-	PAR-1B α	-	SRPK1	-
Abl(252H)	-	CDK7/eyH	-	EphA2	-	Hck act	-	Mer	-	PASK	-	PASK	-	SRPK2	-
Abl(315I)	-	CDK9/eyT1	-	EphA3	-	H1PK1	-	Mer(1246H)	-	PEK	-	PKV2	-	STK25	-
Abl(253F)	-	CHK1	-	EphA4	-	H1PK2	-	Mer(1246N)	-	PDOFR α	-	PKG1 α	-	STK33	-
ACK1	-	CHK2	-	EphA5	-	H1PK3	-	Mer(1268T)	-	PDOFR α (842 V)	-	PKG1 β	-	Syk	-
ALK	-	CHK2(15TT)	-	EphA7	-	IGFIR	-	Mer(1248C)	-	PDOFR α (561D)	-	Plk1	-	TAK1	-
ALK2	-	CHK2(145W)	-	EphA8	-	IGFIR act	-	Mer(1248D)	-	PDOFR β	-	Plk3	-	TAO1	-
ALK4	-	CK1 γ 1	-	EphB2	-	IKK α	-	Mer(1248H)	-	PDK1	-	PRAK	-	TAO2	-
Arg	-	CK1 γ 2	-	EphB1	-	IKK β	-	MINK	-	Phk γ 2	-	PRK2	-	TAO3	-
AMPK α 1	-	CK1 γ 3	-	EphB3	-	IKKe	-	MIKK7 β	-	PBK(β)	-	PhX	-	TBK1	-
AMPK α 2	-	CK1 δ	-	EphB4	-	IR	-	MLCK	-	PBK(γ)	-	PTK5	-	Tec act	-
ARK5	-	CK2	-	ErbB4	-	IR act	-	MLK1	-	PBK(δ)	-	Pyk2	-	TGFBR1	-
ASK1	-	CK2 α 2	-	FAK	-	IRE1	-	Mnk2	-	PBK(1047R)	-	p38 α	-	Tie2	-
Aurom-A	-	CLK1	-	For	-	IRK	-	MRC α	-	PBK α (542K)	-	p38 α 106M	-	Tie2(849W)	-
Aurom-B	-	CLK2	-	Fes	-	IRAK1	-	MRC α β	-	PBK α (545K)	-	p38 β	-	Tie2(Y8978)	-
Aurom-C	-	CLK3	-	FGFR1	-	IRAK4	-	MSK1	-	PBK α 'p65 α	-	p38 γ	-	TLK1	-
Ax1	-	CLK4	-	FGFR1(561M)	-	kk	-	MSK2	-	PBK α 'p65 α	-	p38 δ	-	TLK2	-
Bak	-	cKit	-	FGFR2	-	JAK1	-	MSSK1	-	PBK α 'p65 α	-	Ret	-	TtkA	-
Bmax	-	cKit(816 V)	-	FGFR2(549H)	-	JAK2	-	MST1	-	PBK α 'p65 α	-	Ret(804L)	-	TtkB	-
BRK	-	cKit(816H)	-	FGFR3	-	JAK3	-	MST2	-	PIP4K2 α	-	Ret(804M)	-	TtkC	-
BaSK1	-	cKit(5603)	-	FGFR4	-	JNK1 α 1	-	MST3	-	PIP5K1 α	-	RIPK2	-	TSSK1	-
BaSK2	-	cKit(654A)	-	Fgr	-	JNK2 α 2	-	MST4	-	PIP5K1 γ	-	ROCK-1	-	TSSK2	-
BTK	-	GSK	-	Fit1	-	JNK3	-	mTOR	-	Pim-1	-	ROCK-II	-	Ttk	-
BTK(28H)	-	c-RAF	-	Fx3 83SY	-	KDR	-	mTOR/FKBP12	-	Pim-2	-	Rom	-	TYK2	-
B-Rad	-	cSRC	-	Fx3	-	Lck	-	MnSK	-	Pim-3	-	Ros	-	ULK2	-
B-Rad(599E)	-	DAPK1	-	Fx4	-	Lck act	-	NEK2	-	PKA	-	Rse	-	ULK3	-
CaMKI	-	DAPK2	-	Fms	-	LIMK1	-	NEK3	-	PKB α	-	Rsk1	-	Wee 1	-
CaMKII β	-	DCAMKI,2	-	Fms969C	-	LKB1	-	NEK6	-	PKB β	-	Rsk2	-	WNK2	-
CaMKII γ	-	DDR2	-	Fyn	-	LOK	-	NEK7	-	PKBy	-	Rsk3	-	WNK3	-
CaMKII δ	-	DMPK	-	GCK	-	Lyn	-	NEK9	-	PKC α	-	Rsk4	-	VRK2	-
CaMKII δ	-	DRAK1	-	GCN2	-	LRRK2	-	NEK11	-	PKC β 1	-	SGK	-	Yes	-
CaMKIV	-	DYRK2	-	GRK1	-	MAPK1	-	NLK	-	PKC β II	-	SGK2	-	ZAP-70	-
CDK1/eyB	-	cEF-2K	-	GRK5	-	MAPK2	-	p7086K	-	PKC γ	-	SGK3	-	ZIPK	-
CDK2/eyA	-	EGFR	-	GRK6	-	MAPKAPK2	-	PAK1	-	PKC δ	-	SIK	-		-
CDK2/eyE	-	EGFR(858R)	-	GRK7	-	MAPKAPK3	-	PAK2	-	PKCe	-	Snk	-		-
CDK3/eyE	-	EGFR(861Q)	-	GSK3 α	-	MEK1	-	PAK4	-	PKC η	-	SNRK	-		-

^aAccession number for each kinase is listed in Supporting Information Table S1. ^bHierarchical Kinome inhibitor screen done as described in Methods. p38 α MAPK was the only positive (+) hit (H).

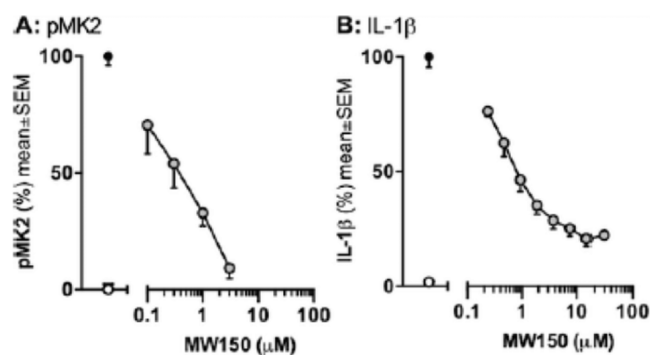


Figure 4. Concentration-dependent cellular activity of MW150. (A) MW150 treatment suppresses the phosphorylation of MK2, a p38 α MAPK substrate whose phosphorylation (activation) is increased in response to LPS activation of glia. Serial dilutions were added to BV2 microglial cells stimulated with 100 ng/mL LPS, and the levels of pMK2 at 1 h determined by ELISA analysis. (B) MW150 treatment attenuates the downstream increase in proinflammatory cytokine production, a mechanism of action pharmacodynamic end point. Levels of IL-1 β at 16 h were determined by ELISA. Data are expressed as percent of maximal activity (=activity after LPS stimulation + control vehicle treatment) and are representative of at least two independent experiments. Open circle = no LPS + veh; black circle = LPS + veh; gray circle = LPS + MW150.

demonstrate that MW150 is able to engage its endogenous kinase target in a relevant physiological state. MK2 is the proximal next step in the intracellular p38 α MAPK signal transduction cascade shown to mediate lipopolysaccharide (LPS)-induced increases in production of proinflammatory cytokines such as interleukin-1 β (IL-1 β). In this context, IL-1 β represents a surrogate pharmacodynamic end point for the p38 α MAPK signal transduction cascade. As shown in Figure 4B, MW150 treatment blocked in a concentration-dependent manner the increased IL-1 β production by activated glia. The IC₅₀ values for these MW150 cellular activities are 332 nM (MK2) and 936 nM (IL-1 β), values which are consistent with the *in vitro* K_i of 101 nM for p38 α MAPK.

As a further derisking of potential off target activities, MW150 was also subjected to a large-scale screen for GPCRs, the largest single target class for approved CNS drugs, in order to address the potential of unanticipated out-of-target-class activity. MW150 showed no agonist or antagonist activity against any of the 166 GPCRs tested in the functional cellular assay (Supporting Information Table S3). The results indicate the extremely low potential for off-target crossover to this major CNS drug target class.

Pharmacological Screens. The United States Food and Drug Administration (FDA) recommends³⁰ testing new molecular entities as potential substrates or inhibitors for a critical set of CYP isoforms that are involved in drug and food metabolism, thereby anticipating dosing, drug–drug interactions, and potential adverse events in future drug development. This is especially true for certain CYP isoforms such as CYP2D6 that are known to encode functional polymorphisms and contribute to pharmacogenetic variance in drug efficacy or toxicology. Paradoxically, when small molecule lead compounds are optimized during multiproperty medicinal chemistry refinement to improve CNS penetrance, an unintended outcome can be increased potential for CYP substrate status.^{25,26} CYP2D6 also can be disproportionately involved in the metabolism of CNS drugs.²⁶ Therefore, CYP2D6

substrate status is a No Go decision point in CNS drug development and is one of the FDA recommended CYPs for screening. While the substrate or inhibitor status for the other recommended CYPs may not be as critical, the outcomes can inform the design of future dosing and adverse pharmacology experiments.

As anticipated based on pharmacoinformatics,^{25,26} MW150 was not found to be a substrate of CYP2D6. Remarkably, MW150 is also not a substrate for any of the other key CYPs recommended for testing in FDA guidance. When screened using the standard assays described in Methods, MW150 exhibited a $T_{1/2}$ > 60 min for all of the recommended CYPs. Positive controls for each of the CYPs and their respective $T_{1/2}$ values were as follows: CYP1A2, ethoxyresorufin ($T_{1/2}$ = 2); CYP2B6, benzphetamine ($T_{1/2}$ = 17); CYP2D6, dextromethorphan ($T_{1/2}$ = 4); CYP3A4, midazolam ($T_{1/2}$ = 4); CYP2C8, paclitaxel, ($T_{1/2}$ = 39); CYP2C9, diclofenac ($T_{1/2}$ = 16); and CYP2C19, omeprazole ($T_{1/2}$ = 21). MW150 was also found not to be a CYP inhibitor when the recommended set of CYP isoforms were examined (Figure 5). The CYP isoform

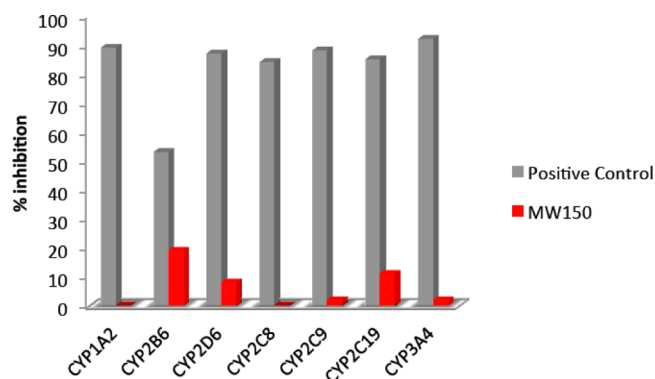


Figure 5. CYP inhibition summary.

positive control inhibitors were as follows: CYP1A2, α -naphthoflavone; CYP2B6, thio-TEPA; CYP2D6, quinidine; CYP2C8, montelukast; CYP2C9, sulfaphenazole; CYP2C19, (+)-*N*-3-benzylmivanol; CYP3A4, ketoconazole. These remarkable results from both CYP substrate and CYP inhibitor analyses are positive indicators of lowered risk for use of MW150 in future *in vivo* drug combination studies which are expected for complex disease investigations.

The aggregate effect of CYP-based status was next evaluated in standardized liver microsome assays. Testosterone was used as a validation control for both rat and human microsomal preparations, and percent remaining of test compounds was determined by LC-MS based on the peak area ratio to the internal standard propranolol. MW150 has a human liver microsome stability $T_{1/2}$ > 60 min and a rodent liver microsomal $T_{1/2}$ = 43 \pm 4 min. The intrinsic clearance (CL_{int}) was estimated as 0.02 \pm 0.00 mL/min/mg protein. We concluded that the liver microsome stability was acceptable for additional pharmacological studies.

A quantitative cellular pharmacology parameter that is critical for CNS targeting is the standard assay used to filter drug candidates for acceptable cell permeability and efflux pump substrate status. Most small molecule drugs predominately move via passive diffusion through cellular membranes that comprise tissue barriers. However, if the drug is an efflux pump substrate, it is removed and eventually excreted from the body.

Table 4. Caco-2 Permeability/P-gp Substrate Summary for MW150

sample	concn (μM)	time (h)	mean A \rightarrow B P_{app} (10^{-6} cm s^{-1}) ^a	mean B \rightarrow A P_{app} (10^{-6} cm s^{-1}) ^a	efflux ratio ^b	notes
MW150	5	2	33.5	31.2	0.9	high permeability
MW150 + valsopodar	5	2	27.6	23.0	0.8	not a P-gp substrate

^aApparent permeability. ^b $P_{\text{app}}(\text{B} \rightarrow \text{A})/P_{\text{app}}(\text{A} \rightarrow \text{B})$.

Table 5. MDCK Permeability/BCRP Substrate Summary for MW150

sample	concn (μM)	time (h)	mean A \rightarrow B P_{app} (10^{-6} cm s^{-1}) ^a	mean B \rightarrow A P_{app} (10^{-6} cm s^{-1}) ^a	efflux ratio ^b	notes
MW150	5	2	20.7	25.1	1.2	high permeability
MW150 + Ko143	5	2	26.1	24.3	0.9	not a BCRP substrate

^aApparent permeability. ^b $P_{\text{app}}(\text{B} \rightarrow \text{A})/P_{\text{app}}(\text{A} \rightarrow \text{B})$.

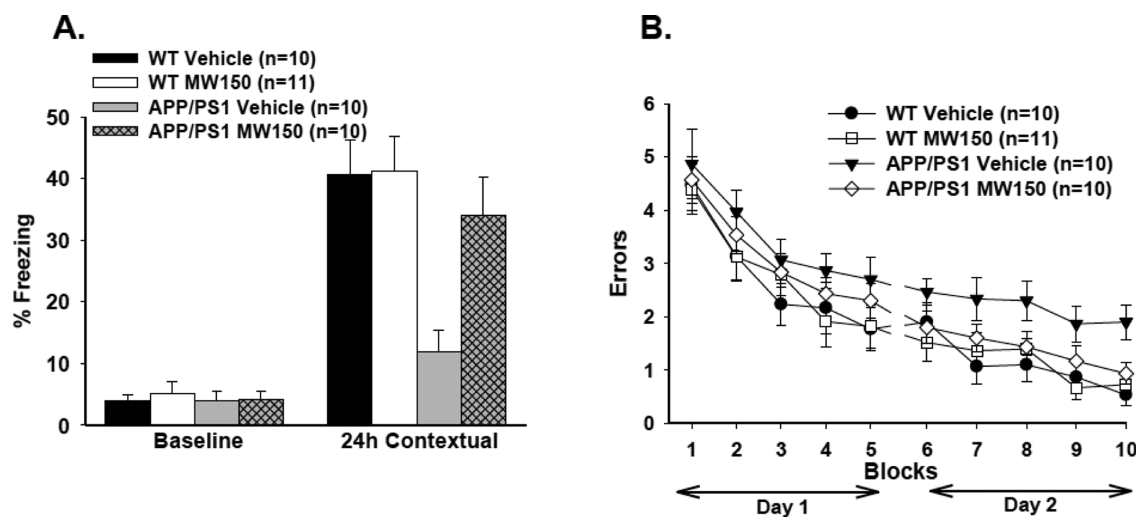


Figure 6. MW150 treatment suppresses associative and spatial memory deficit in APP/PS1 Tg mice. Daily oral administration of either saline or MW150 (2.5 mg/kg) was done from age 8 weeks to 3–4 months. Associative and spatial memories were then assessed, respectively, through (A) contextual fear memory and (B) RAWM. Saline treated APP/PS1 mice exhibited cognitive deficits for both types of memory compared to saline treated-type (WT) mice, as evidenced by a significantly lower percent of freezing during assessment of fear memory, and by higher number of errors in the RAWM task. However, treatment of APP/PS1 mice with MW150 resulted in suppression of the deficits, as seen by the percent of freezing and RAWM performance indistinguishable from that of WT mice.

Poor permeability due to molecular properties and efflux pump substrate status can individually or in combination with other factors contribute to a drug's inadequate CNS penetration. Therefore, MW150 was subjected to both the classical Caco-2/P-gp screening system and the more recently developed MDCK/BCRP screening assay.

The data summarized in Table 4 demonstrate that MW150 has high cell permeability and is not a substrate for P-gp efflux pump. For apical to basolateral (A \rightarrow B) permeability, the test agent is added to apical side and permeation determined by LC/MS/MS measured on basolateral side; the opposite is done for (B \rightarrow A). P-gp substrate status is then determined by measuring the effect of the standard inhibitor 1 μM valsopodar on bidirectional flux. The percent recovery of MW150 is 71% and 61%, respectively.

As shown in Table 5, MW150 also has high cell permeability for MDCK cells and is not a substrate for the BCRP efflux transporter. The standard inhibitor Ko143 (10 μM) was used to probe bidirectional flux in this assay. Percent recovery of MW150 was 66% and 67%, respectively.

The results from molecular and cellular property screening assays for MW150 warranted progression to in vivo pharmacological screens. First, a preliminary screen for oral bioavailability potential was done in rat. Pharmacokinetic

parameters were determined after intravenous (iv) and oral (po) administration at 5 mg/kg. Animals were fasted prior to MW150 administration and up to 4 h post administration. All animals showed normal activity during the study. The concentration of MW150 in plasma samples was determined by LC-MS/MS, and the parameters estimated by a non-compartmental analysis. The screening data show that MW150 has a half-life in excess of 3 h and an oral bioavailability of >50%. Second, the pharmacokinetic screening results were used in the design of a brain-to plasma ratio screen for tissue penetration potential. MW150 was administered at the same 5 mg/kg dose and levels measured in plasma and brain samples 3 h post administration. The estimated brain/plasma ratio of >0.9 indicates that MW150 is able to distribute across the blood-brain barrier. Clearly, MW150 has attractive oral bioavailability potential, warranting a full dose dependent kinetic analysis in future investigational new drug development investigations.

Prior to analysis for efficacy, MW150 was also screened in a modified SHIRPA test paradigm⁶ to minimize the impact of unanticipated adverse pharmacology and unintended influences on the interpretation of behavioral studies. This consensus approach to filtering for frank adverse pharmacology prior to candidate selection provides a degree of derisking for future investigational new drug enabling studies and allows fuller

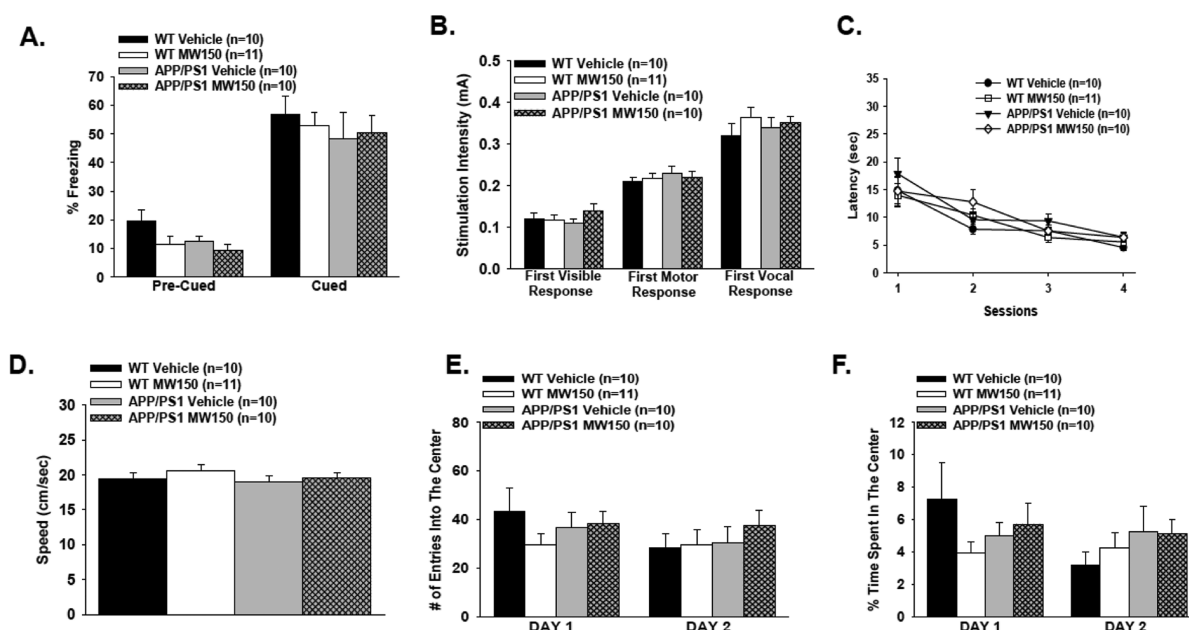


Figure 7. Control behavioral analyses for MW150 suppression of associative and spatial memory deficits in APP/PS1 transgenic mice. No difference was detected between groups when tested for cued fear memory (A), sensory threshold (B), visual-motor-motivational deficits with the visible platform test (speed and time to the platform are shown in (C) and (D), respectively), and exploratory behavior, as shown by a similar percentage of time spent in the center compartment (E) and the number of entries into the center compartment (F).

interpretation of animal behavior studies used as an efficacy end point. Briefly, C57BL/6 mice were administered saline (control) or MW150 (50 and 150 mg/kg, 20- and 60-fold above the efficacy dose) and clinical observation documented. Normal individual variances among mice in all groups were observed in total distance traveled or center versus edge occupancy, but no differences or adverse events were detected among saline or MW150 treated mice over a 24 h period of observation.

We conclude that MW150 is a chemically stable and orally bioavailable p38 α MAPK inhibitor that exhibits excellent cell permeability, absence of efflux pump and CYP liabilities, adequate metabolic stability and possessing minimal risk for adverse pharmacology liabilities. The aggregate outcomes, therefore, justified *in vivo* evaluation of efficacy.

Behavior as Pharmacodynamic Test of *in Vivo* Efficacy. Memory loss is the clinical hallmark of AD. Most importantly for drug discovery, the current FDA approved AD drugs used the attenuation of memory loss as a qualifying end point. We therefore decided to use a behavioral assessment of memory as the initial pharmacodynamic readout for MW150 efficacy. Two distinct AD-relevant mouse models were tested: the APP/PS1 transgenic (Tg) mouse and the APP^{NLh/NLh} \times PS^{P264L/P264L} knock-in (KI) mouse. Both models show synaptic dysfunction and cognitive deficits.^{6,27} The APP/PS1 Tg model overexpresses amyloid-beta ($A\beta$). It is an amyloid deposition model in which selective p38 α MAPK inhibition has been linked to attenuation of long-term potentiation (LTP) and cognitive dysfunction brought about by amyloid-beta ($A\beta$) stress.⁶ In contrast, the genetic APP/PS KI model uses endogenous promoters with no overexpression of the amyloid precursor protein (APP). It reflects physiological levels of APP and is an aging model that allows testing at either early or late stage pathology progression.²⁷

The Tg mouse model was tested in a preventative paradigm, as previously described.⁶ Because both associative and spatial

memory are known to be affected in AD patients, we tested the effects of MW150 on contextual fear learning, a hippocampus-dependent task assessing associative memory, and in the two-day RAWM task that assesses spatial memory. Briefly, wild type (WT) and APP/PS1 littermate mice were treated with MW150 (2.5 mg/kg, oral, daily) or vehicle starting at 8 weeks of age and continuing until 3–4 months when cognitive impairment is present. Behavioral assessments were done with the radial arm water maze (RAWM) and contextual fear conditioning tests as described.⁶ MW150 treatment improved the Tg mice performance in both cognitive tests (Figure 6).

The specificity of a physiological axis response to therapeutic intervention is key to relevance of an animal model pharmacodynamic end point to future clinical studies. Therefore, it is worth noting additional pharmacodynamic effects of MW150 that provide a firmer foundation and translational value. Specifically, MW150's behavioral effects are selective and consistent with hippocampal mediated mechanisms. For example, treatment with MW150 did not affect the performance of WT mice (Figure 6), consistent with MW150 treatment altering disease-relevant mechanisms instead of a more general effect on memory. Further, there was no effect on cued fear memory, a hippocampus-independent type of memory. Other analyses reinforce the disease relevant physiological axis (Figure 7). For example, the sensory threshold was similar among different groups of mice, indicating there was no modification of the ability to perceive the shock (Figure 7). Additionally, MW150 treatment did not influence the visible platform task, which assesses sensory, motor, and motivational mechanisms, and did not influence open field tests, which assess locomotor activity and anxiety (Figure 7C–F). Finally, the effect of MW150 treatment is dose dependent for behavior end points (Supporting Information Figure S2).

The second AD-relevant mouse model used to test MW150 intervention was in older mice where cognitive deficits are already present. The humanized APP/PS1 KI mouse model is

driven by endogenous promoters of the APP and PS1 genes, generating progressive pathology without overproduction. The KI mice exhibit a spatial memory deficit in the RAWM by the age of 11 months. The deficits can be attenuated by pharmacological interventions that target cognitive dysfunction brought about by excessive proinflammatory cytokine production.²⁸ Treatment of 11–12 month old mice with MW150 (2.5 mg/kg, ip, daily for 14 days) suppressed the cognitive impairment, assessed by RAWM 3 days after the last administration. The MW150-treated mice exhibit RAWM behavior indistinguishable from WT mice (Figure 8).

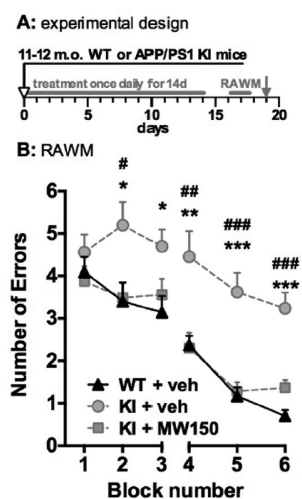


Figure 8. MW150 treatment suppresses spatial memory deficit in APP/PS1 knock-in (KI) mice. MW150 administration (A) to APP/PS1 KI mice (2.5 mg/kg; ip, daily for 14 days; $n = 11$, gray squares) suppressed cognitive deficits (B) seen in APP/PS1 KI mice treated with vehicle (gray circles, $n = 12$) and was indistinguishable from WT mice treated with vehicle (black triangles, $n = 14$). Mice were tested in a 2-day RAWM assay of spatial reference memory starting 3 days after the last treatment. Cognitive deficits in the KI mice treated with vehicle were evidenced by a significantly higher number of errors in RAWM performance compared to KI mice treated with MW150 ($^{\#}p < 0.05$, $^{\#\#}p < 0.005$, $^{\#\#\#}p < 0.001$) or WT mice treated with vehicle ($^*p < 0.05$, $^{**}p < 0.005$, $^{***}p < 0.001$).

From the perspective of end points that reflect the scientific foundation of currently approved AD therapeutics, the independently obtained results in two distinct pathology progression models demonstrate the ability bring about pharmacological efficacy with MW150 repeat dosing. Further, the results in a battery of behavioral tests are consistent with a true hippocampus-dependent mechanism of action in attenuation of memory deficits. Repeat dosing with MW150 did not bring about any observed adverse events within the targeted physiological axis or control behaviors in aged or diseased animals. The selective improvement in cognitive behavior was also brought about with no effect on amyloid plaque load (Supporting Information Figure S3).³¹

SUMMARY AND CONCLUSIONS

MW150 is a unique protein kinase inhibitor with in vivo efficacy in two distinct AD relevant models at a low dose with repeat administration and no observed adverse events in aged mice. Behavior is a complex and technically challenging end point. This is one motivation for our performing efficacy testing in independent animal models of AD related pathophysiology

and for examination of diverse behavioral controls in the experimental design. Overall, the results summarized here indicate a selective effect of MW150 intervention on cognitive performance via a hippocampus-dependent mechanism of action, consistent with prevailing perspectives on human dementia progression and drug regulatory approval paradigms.

We have described a pharmacological intervention relationship for a comparatively simple single stressor–single kinase–neuropathophysiology paradigm, but the availability of MW150 provides an embarkation point for placing into context the various other roles hypothesized for activated p38 α MAPK in complex CNS disease phenotypes. For example, MW150 is currently being used to address the potential of attenuating neuropsychiatric disorder phenotypes involving neuronal p38 α MAPK activation. In the long term, extended application of this unique protein kinase inhibitor to diverse CNS pathophysiology progression mechanisms might better inform us about which p38 α MAPK mediated dysfunctions are more tractable for intervention and are more clinically relevant.

MW150 is efficacious when administered either before full-fledged pathology is evident or after pathology is already present, reflecting potential for use in either a prevention mode or disease treatment mode. The promising outcomes with repeat dosing administration might be a reflection of MW150's pharmacological profile and protein kinase isoform selectivity, or it might reflect parallel pharmacological action on stress activated glia and neurons in close proximity within the synaptic pathophysiology unit. While both possibilities are intriguing and desired, their relative contributions cannot be fully interpreted based on the results reported here. Regardless, a degree of derisking for future IND enabling analyses and a potential for use in a polypharmacy environment, which characterizes complex CNS disease interventions, are evident in the battery of pharmacological screen outcomes such as lack of substrate status for key CYPs defined by regulatory guidelines, good bioavailability potential, promising CNS exposure, and no observed frank adverse events.

Target selectivity is demonstrated by a variety of approaches, including large-scale kinome and GPCR screens in conjunction with cellular target engagement and surrogate pharmacodynamic end points. The structural basis of MW150 kinome and isoform selectivity appears to reside in a combination of two key interactions that engage the p38 α MAPK hinge region and a proximal hydrophobic pocket. Hinge region H-bond engagement is a common theme among the diverse chemical classes of p38 α MAPK inhibitors that exhibit in vivo function.^{3,5,6,9} MW150 fulfills this role through use of the pyridine substituent nitrogen atom. No localized conformational changes are observed with MW150 binding to the hinge region, such as the glycine flip observed with other promising p38 α MAPK inhibitors. The finding is consistent with previous work⁶ that showed this localized conformational change in the kinase is not required for selective p38 α MAPK inhibition. A second interaction of MW150 with p38 α MAPK is occupancy of a proximal hydrophobic pocket by a vicinal 2-naphthyl substituent. This pocket is not exploited by ATP, in contrast to the hinge region engagement which is used by ATP. The shape and space filling features of the 2-naphthyl group allow extensive filling of the hydrophobic pocket. A similar pocket is found in other p38MAPK isoforms and a limited set of other kinases, but the shape and properties of the hydrophobic pockets in other kinases do not appear as accommodating of the 2-naphthyl substituent. The pocket accessibility and space

filling features of the 2-naphthyl substituent of MW150, therefore, appear to add a structure based selectivity filter. Additional interactions observed among other p38 α MAPK inhibitors, such as those resulting in DFG-out conformations, are not observed in the high-resolution structure presented here. This finding is consistent with previous work^{2,3,6} that showed the DFG-out conformation does not always correlate with kinase inhibition and is not required for isoform selectivity. Overall, the presence of the vicinal pyridinyl and 2-naphthyl substituents in the context of the pyridazine scaffold is the most parsimonious explanation of what MW150 features provide selective target engagement, while MW150 molecular properties²⁵ and specific aspects of its first pass metabolism²⁶ appear to drive bioavailability and pharmacological exposure in order to deliver the highly selective in vivo efficacy.

In conclusion, the results presented here add to a body of knowledge that raises the rational possibility of p38 α MAPK inhibitor drugs for CNS indications might be one in which efficacy, either in a palliative or disease modifying mode, is a reasonable anticipation. Current perspectives on p38 α MAPK inhibitor drugs are influenced by perceived failures in some disease indication areas even while others continue to show promising outcomes.^{32,33} In this regard, it should be noted that drug development termination at the clinical trials stage is not equivalent to efficacy failure. For example, termination in clinical development can be due to business decisions on the part of pharmaceutical companies or to regulatory issues such as a trial achieving efficacy but not surpassing current standards of care. Such terminations are distinct from failure to reach the trial efficacy goals. In this context, the approved AD drugs are acetylcholinesterase inhibitors and most recent and ongoing clinical trials target the amyloid pathway and generally fail to reach efficacy. Therefore, an established standard for attenuation of pathophysiology progression remains a future goal for the AD field. Additionally, the gap in CNS kinase inhibitor drug development²⁵ remains. In this context, it is clearly worth pursuit of p38 α MAPK inhibitors similar to MW150 as CNS therapeutic candidates. Further, the promising pharmacological profile of MW150 also makes it a potential complementary intervention that might enhance outcomes from prevailing AD therapeutic development approaches or be used in combination therapies for this complex disease.

METHODS

Synthesis and Characterization of MW150 for Biological Studies (Scheme 1). The experimental detail for the title compound MW150 is presented here. The synthesis of additional compounds used in the investigation are presented in the Supporting Information.

***N*-Methoxy-*N*-methyl-2-naphthamide (2).** A mixture of 2-naphthoyl chloride (1, 35 g, 0.18 mol) and *N,N*-dimethylhydroxylamine hydrochloride (21.5 g, 0.22 mol) in dichloromethane (1L) was stirred, cooled in an ice bath, and treated with diisopropylethylamine (58 g, 0.45 mol, 81 mL) dropwise over 30 min. The mixture was warmed to 20 °C over 2 h then stirred an additional 1 h. The solvents were evaporated, and the residual solid was dissolved in ethyl acetate (500 mL) and water (500 mL). The organic layer was separated and washed with 1 N HCl (300 mL), water (300 mL), and brine (200 mL). The organic phase was dried (Na₂SO₄) and evaporated to leave the product as a light tan oil (2, 39.5 g, 100%). Mass (ESI) *m/z* 216 (M + H)⁺.

1-(Naphthalen-2-yl)-2-(pyridin-4-yl)ethan-1-one (3). A solution of 4-picoline (15.6 g, 168 mmol, 16.2 mL) in anhydrous THF (1 L) under nitrogen atmosphere at -78 °C was treated with a solution of freshly prepared LDA [from a solution of diisopropyl amine (25.4 g, 252 mmol, 35.4 mL)] in THF (140 mL) under nitrogen atmosphere

in an ice bath treated with *n*-butyllithium solution (2.5 M in hexanes, 100 mL, 252 mmol and stirred for 30 min) over 30 min via cannula. The mixture was stirred at -78 °C for 1 h and was treated with *N*-methoxy-*N*-methyl-2-naphthamide (2, 40 g, 186 mmol) in THF (160 mL) dropwise over 1.5 h while ensuring the temperature was maintained at or below -75 °C. The mixture was then allowed to warm to 20 °C over 4 h and stirred an additional 16 h at this temperature. Saturated ammonium chloride solution (100 mL) was added to the mixture and allowed to stir 30 min. The solvents were evaporated in vacuo to approximately 20% of the original reaction mixture volume and the residue was dissolved in ethyl acetate (1 L) and water (600 mL). The organic layer was separated and washed with water (600 mL). The product was extracted from the organic layer with 1 N HCl (2 × 300 mL). The combined acid extracts were neutralized with solid sodium bicarbonate to pH = 8. The precipitated product was filtered, washed with water (2 × 50 mL), and dried under vacuum for 16 h to leave a light yellow solid (3, 34.5 g, 83%). ¹H NMR (300 MHz, CDCl₃) δ 8.58 (dd, *J* = 4.4, 1.8 Hz, 2H), 8.53 (s, 1H), 8.05 (dd, *J* = 8.5, 1.8 Hz, 1H), 8.00–7.84 (m, 3H), 7.66–7.55 (m, 2H), 7.25 (m, 2H), 4.43 (s, 2H). Mass (ESI) *m/z* 248 (M + H)⁺. LC/MS R_t = 3.37 min.

Ethyl 4-(Naphthalen-2-yl)-4-oxo-3-(pyridin-4-yl)butanoate (4). A solution of 1-(naphthalen-2-yl)-2-(pyridin-4-yl)ethan-1-one (3, 34 g, 138 mmol) in anhydrous 1,4-dioxane (750 mL) under nitrogen atmosphere was treated with sodium hydride (60% in mineral oil, 6.8 g, 170 mmol) and stirred for 1 h with occasional venting to prevent hydrogen accumulation. The mixture, which had a yellow precipitate, was treated with ethyl 2-bromoacetate (28 g, 170 mmol, 18 mL) and stirred for 18 h. A solution of saturated ammonium chloride (100 mL) was added and the mixture stirred for 30 min. The solvents were evaporated to approximately 80% of the original volume and the residue was diluted with ethyl acetate (600 mL) and water (400 mL). The mixture was filtered through Celite (ethyl acetate wash) to remove a small amount of yellow precipitate. The organic layer was separated and the product was extracted with 1 N HCl (4 × 100 mL). The combined acid extracts were neutralized with solid sodium carbonate (pH = 9) and the product was extracted with ethyl acetate (2 × 300 mL). The combined organic extracts were washed with brine, dried over Na₂SO₄ and evaporated. The crude residue (26 g) was used in the next step without purification or characterization.

6-(Naphthalen-2-yl)-5-(pyridin-4-yl)-4,5-dihydropyridazin-3(2H)-one (5). A solution of ethyl 4-(naphthalen-2-yl)-4-oxo-3-(pyridin-4-yl)butanoate (4, 26 g, 51 mmol) in ethanol (175 mL) and acetic acid (8 mL) was treated with hydrazine hydrate (110 g, 1.2 mol, 110 mL) and refluxed for 20 h. A beige precipitate formed. The mixture was cooled to 20 °C and filtered to collect the product which was washed with ice cold methanol (40 mL) and acetonitrile (40 mL) and air-dried to leave a cream colored powder (5, 15.0 g, 36% for two steps). ¹H NMR (300 MHz, CDCl₃) δ 8.76 (bs, 1H), 8.57 (d, *J* = 5.3 Hz, 2H), 7.98 (dd, *J* = 8.5, 1.8 Hz, 1H), 7.95 (s, 1H), 7.85 (d, *J* = 8.5 Hz, 1H), 7.86–7.76 (m, 2H), 7.55–7.46 (m, 2H), 7.21 (dd, *J* = 4.4, 1.2 Hz, 2H), 4.68 (d, *J* = 6.5 Hz, 1H), 3.10 (dd, *J* = 17.0, 7.7 Hz, 1H), 2.90 (dd, *J* = 17.0, 1.8 Hz, 1H). Mass (ESI) *m/z* 302 (M + H)⁺. LC/MS R_t = 3.11 min.

6-(Naphthalen-2-yl)-5-(pyridin-4-yl)pyridazin-3(2H)-one (6). A round-bottom flask equipped with a stir bar was charged with 6-(naphthalen-2-yl)-5-(pyridin-4-yl)-4,5-dihydropyridazin-3(2H)-one (5, 14.5 g, 48 mmol), water (7 mL), and DMSO (250 mL). The mixture was stirred and treated with *N*-bromosuccinimide (42 g, 233 mmol). The reaction mixture turned yellow and a slight exotherm was noted while all solid contents went into solution. After stirring for 20 h, the mixture was poured into a stirring solution of water (1 L) and saturated sodium bicarbonate solution (500 mL) at such a rate that effervescence remained under control. The white precipitate that formed was collected on a glass frit, washed with water (2 × 50 mL), and air-dried to leave product (6, 13.9 g, 97%). ¹H NMR (300 MHz, CDCl₃) δ 11.13 (bs, 1H), 8.55 (bs, 2H), 7.80 (dd, *J* = 9.1, 2.1 Hz, 1H), 7.76–7.68 (m, 3H), 7.55–7.45 (m, 2H), 7.16 (dd, *J* = 8.8, 2.0 Hz, 1H), 7.09 (d, *J* = 5.9 Hz, 2H), 7.05 (s, 1H). Mass (ESI) *m/z* 300 (M + H)⁺. LC/MS R_t = 2.88 min.

6-Bromo-3-(naphthalen-2-yl)-4-(pyridin-4-yl)pyridazine (7). A round-bottom flask equipped with a stir bar was charged with phosphorousoxybromide (29 g, 102 mmol) and anhydrous acetonitrile (310 mL). The mixture was stirred until all solids were dissolved. To this solution was added 6-(naphthalen-2-yl)-5-(pyridin-4-yl)pyridazin-3(2H)-one (6, 13.3 g, 44.5 mmol), and the mixture was heated to reflux for 18 h. The reaction mixture was cooled in an ice bath, treated with ice (150 g), and stirred for 1 h. The reaction mixture volume was reduced to 50% of the original volume by evaporation under vacuum. The residual mixture was neutralized with solid sodium carbonate (pH = 9), and the product was extracted with ethyl acetate (2 × 100 mL). The combined organic layers were washed with brine (100 mL), dried (Na₂SO₄), and evaporated. The crude product was purified by silica gel (EM Baker, 230–400 mesh) chromatography eluted with a gradient of ethyl acetate in hexanes (1:1 to 9:1) to leave the product as a light beige solid (7, 9.6 g, 60%). ¹H NMR (300 MHz, CDCl₃) δ 8.59 (dd, 2H, *J* = 4.3, 1.8 Hz), 8.03 (d, *J* = 1.4 Hz, 1H), 7.85–7.65 (m, 3H), 7.72 (s, 1H), 7.58–7.47 (m, 2H), 7.33 (dd, 1H, *J* = 8.5, 1.8 Hz), 7.15 (dd, 2H, *J* = 4.7, 1.8). Mass (ESI) *m/z* 364 (M + H)⁺. LC/MS R_t = 3.71 min.

6-(4-Methylpiperazin-1-yl)-3-(naphthalen-2-yl)-4-(pyridin-4-yl)pyridazine (8 = MW150). A solution of 6-bromo-3-(naphthalen-2-yl)-4-(pyridin-4-yl)pyridazine (7, 11.5 g, 32 mmol) in 95% ethanol (170 mL) was treated with 1-methylpiperazine (15.9 g, 158 mmol, 18 mL) and heated to reflux for 18 h. Upon cooling to 20 °C, approximately 90% of the ethanol was evaporated under reduced pressure. The residue was dissolved in ethyl acetate (200 mL) and aqueous saturated sodium bicarbonate solution (150 mL). The organic layer was separated and washed with water (2 × 200 mL). Minutes after the second water wash, the product precipitated from the organic layer while still in the separatory funnel. The solid was collected on a medium glass frit via suction filtration, washed with ethyl acetate (2 × 20 mL), and dried under vacuum (1 mm Hg) at 50 °C for 12 h. The desired material 8 (MW150) was obtained as a pale yellow solid (11.5 g, 94%). ¹H NMR (CDCl₃, 500 MHz) δ 8.53 (dd, *J* = 1.7, 4.4 Hz, 2H), 7.92 (s, 1H), 7.78 (dd, *J* = 1.8, 7.7 Hz, 1H), 7.71–7.67 (m, 2H), 7.47–7.41 (m, 2H), 7.34 (dd, *J* = 1.7, 8.5 Hz, 1H), 7.13 (dd, *J* = 1.7, 4.4 Hz, 2H), 6.86 (s, 1H), 3.83 (t, *J* = 4.7, 4.7 Hz, 4H), 2.62 (t, *J* = 5.0, 5.1 Hz, 4H), 2.39 (s, 3H). Mass (ESI) *m/z* 382.20 (M + H)⁺. HRMS (mass) calculated for C₂₄H₂₃N₅: 381.1953. Found: 381.19603. Elemental analysis calculated (%) for C₂₄H₂₃N₅: C, 75.56; H, 6.08; N, 18.36. Found C, 73.70 H, 6.31; N, 17.93. LC/MS R_t = 2.58 min, mp 188.5–189 °C.

6-(4-Methylpiperazin-1-yl)-3-(naphthalen-2-yl)-4-(pyridin-4-yl)pyridazine hydro chloride hydrate (9). In a round-bottom flask fitted with condenser and dry tube, compound 6-(4-methylpiperazin-1-yl)-3-(naphthalen-2-yl)-4-(pyridin-4-yl)pyridazine (8, 9.1 g, 23.8 mmol) was suspended in 95 mL of anhydrous isopropanol (99.5%, Aldrich) and heated to 89 °C with stirring until dissolved. To the resulting solution, ultrapure HCl (12 N, JT Baker Ultrex II, product 6900-05) (2.5 equiv, 5.1 mL, 59.63 mmol) was added in-portion, inducing formation of solids in suspension. The resulting solution was stirred at 81 °C for 10 min, cooled to ambient temperature, and placed on an ice-bath for 2.5 h. The suspension was then transferred to 4 °C for an additional 10 h. The resulting yellow precipitate was filtered on a medium frit sintered glass funnel using a house vacuum, immediately washed three times with ice-cold anhydrous isopropanol (3 × 35 mL), followed by ice-cold anhydrous ether (3 × 50 mL), and air-dried using house vacuum for 7 h. The product was then dried in a glass desiccator containing silica gel in vacuo until the compound gave a constant weight. Product 9 obtained as a yellow powder (11.12g, 96%), HPLC purity > 98% (LC/MS). ESI *m/z* (MeOH) 382.2 (M+H)⁺. ¹H NMR (500 MHz, MeOD) δ 8.75 (dd, *J* = 1.5, 5.0 Hz, 2H), 7.96 (s, 1H), 7.91–7.83 (m, 6H), 7.58–7.52 (m, 2H), 7.38 (dd, *J* = 1.8, 8.4 Hz, 1H), 4.86 (m, 2H), 3.71 (m, 2H), 3.57 (m, 2H), 3.28 (m, 2H), 3.01 (m, 3H). HRMS (mass) calculated for C₂₄H₂₃N₅: 381.19535. Found: 381.1955. Elemental analysis calculated (%) for C₂₄H₂₉Cl₃N₅O₂: C, 58.78; H, 5.96; N, 14.28; Cl, 14.46; O, 6.52. Found: C, 58.89 H, 5.89; N, 14.15; Cl, 14.27; O, 7.05. mp 240 °C, decomposes.

Aqueous solubility was determined by Absorption Systems as previously described.⁶ Briefly, 1 mg of MW150 powder was combined with 1 mL of buffer to make a 1 mg/mL mixture and shaken on a Thermomixer overnight at room temperature (22 °C). The pH of the water was also measured before addition of test compound and after overnight equilibration. The samples were then passed through a 0.2 μm PTFE syringe filter and diluted in duplicate 10-, 100-, and 10 000-fold into a mixture of 1:1 buffer: acetonitrile prior to analysis, and assayed by LC-MS/MS using electrospray ionization against standards prepared in a mixture of 1:1 assay buffer/acetonitrile. Standard concentrations ranged from 1.0 μM down to 3.0 nM.

The acid dissociation constant (pK_a) of MW150 was determined by pION Inc. (Billerica, MA) using both potentiometric and UV methods as previously described.⁶ The cosolvent was methanol, experimental pH range was 1.7–12.8, assay vials were thermostated at 25 °C, and ionic strength was 0.15 M KCl. Eight titrations were used to calculate the pK_a using the Yasuda–Shedlovsky technique.³⁴ Quality control and calibrants used were phosphate, 0.5 N KOH, 0.5 N HCl, and the FDA approved drug quinine. The pK_a values obtained from spectrophotometric experiments are in excellent agreement with those derived from potentiometric titrations.

Chemical stability was determined by Absorption Systems (Exton, PA) as described previously.⁶ Briefly, at a final concentration of 0.001 M at neutral (pH 7), 0.1 N NaOH (pH 13.0), or 0.1 N HCl (pH 1.0) at 37 °C, conditions were tested, with samples taken for analysis at 0, 1, 3, 6, and 24 h. MW150 is chemically stable over a wide range of pH.

Crystallography and Structure Determination. Experiments involving target–drug complex formation, data collection, and data processing were done using the standard operating protocol as validated previously⁶ for the determination of atomic resolution ligand–kinase crystal structures. Protein purification⁶ was done using a combination of affinity-based adsorption chromatography (HisTrap; GE Healthcare), gel filtration (HiPrep 26/10 column; GE Healthcare), and ion exchange chromatography (Q Sepharose; GE Healthcare).

In Vitro Activity. Large-scale screens for off-target activity within the kinome were done using the hierarchical screening protocol described previously.⁶ MW150 was screened in a commercially performed (Millipore Profiler, now Eurofins) high throughput system that included 301 protein and lipid kinases representative of all major kinome branches as well as isoforms of individual families. Substrates were optimized for each kinase. The final concentration of MW150 in the profiler screen (20 000 nM) was achieved by serial dilution of a DMSO stock solution to the final assay concentration in 2.0% DMSO/Tris buffer. Preliminary hits from the profiler screen (<40% kinase activity remaining) were validated as true positives or false hits by a follow-up determination of an IC₅₀ value. An estimated K_i value was determined on confirmed positives with IC₅₀ < 1000 nM. A similar hierarchical approach⁶ was used for functional GPCR agonist and antagonist screens. The GPCR Profiler screen uses real-time calcium flux FLIPR assay. MW150 was tested at 12 500 nM for agonist and 10 000 nM for antagonist activity. Similar to kinase profiler, apparent hits were determined as true positive or false hits by follow-up IC₅₀ determination compared to a control agonist or antagonist for the given GPCR. Details are provided in Supporting Information Table S3.

MW150 was tested for CYP substrate status with the standard FDA recommended series of CYPs using the commercial service provider CEREP (Redmond, WA). MW150 (0.1 μM) was tested in duplicate against CYP1A2, CYP2B6, CYP2D6, CYP2C8, CYP2C9, CYP2C19, and CYP3A4. For each screen, a reference compound was at a concentration of 0.1 μM. T_{1/2} was estimated from the slope of the linear portion of the curve for compound remaining (%) versus time, assuming first order kinetics. Inhibitor status of MW150 with the FDA recommended CYPs (CYP1A2, CYP2B6, CYP2D6, CYP2C8, CYP2C9, CYP2C19, and CYP3A4) was done by Absorption Systems, Inc. (Exton, PA) using a standardized human liver microsomal assay. Briefly, MW150 (10 μM) and a CYP-specific probe substrate (at concentration approximating its K_m value) were incubated at 37 °C for 10–30 min, reactions terminated and metabolites monitored by LC-MS/MS. Positive controls for each CYP were performed separately

using a known inhibitor. Monoamine oxidase (MAO) inhibition status of MW150 was determined by Cypotex (Watertown, MA) by assaying the ability of MW150 (0.01–25 μM) to inhibit the conversion of probe substrate kynuramine, using the nonselective MAO inhibitor, tranylcypromine, as a positive control.

Human plasma protein binding using rapid equilibrium dialysis was done by Absorption Systems (Exton, PA) in a 96-well dialysis plate assay for plasma protein binding. Briefly, plasma (300 μL) containing the test and control articles was loaded into dialysis plate wells and PBS (500 μL) added to each corresponding receiver chamber, incubation done for 4 h at 37 $^{\circ}\text{C}$, and aliquots of both chambers processed and analyzed by LC-MS/MS.

Stability analyses in human liver microsome (HLM) and rat liver microsome (RLM) assays were performed by Absorption Systems (Exton, PA). Briefly, MW150 (1 μM) in 100 mM potassium phosphate, pH 7.4, 5 mM magnesium chloride was incubated at 37 $^{\circ}\text{C}$ in a shaking water bath after initiation of reaction by the addition of 1 mM NADPH, and time points taken at 30, 45, and 60 min. Reaction termination was done by addition of an equal volume of acetonitrile containing 0.1% formic acid, samples processed and analyses by LC-HRMS to monitor loss of parent compound and appearance of metabolites. Percent of remaining parent compound is calculated relative to $t = 0$ min, with assays being done in duplicate. The validation control (testosterone for human and rat) was assayed by LC-MS/MS using electrospray ionization. The peak area response ratio to internal standard propranolol at each time point was compared to the response ratio at time 0 to determine the percent remaining. Graph Pad (San Diego, CA) was used to calculate the half-life, and data were fit to a single-phase exponential decay equation. The intrinsic clearance (CL_{int}) was calculated based on $CL_{\text{int}} = k/D$, where k is the elimination rate constant and D is protein concentration.

Cell Based Activity. MW150 inhibition of lipopolysaccharide (LPS)-induced responses was tested in the murine microglial BV-2 cell line as previously described.⁶ Briefly, cells were treated with either saline vehicle control or 100 ng/mL LPS (*Salmonella enterica* serotype typhimurium, Sigma-Aldrich: EU/mg of LPS is 600 000), in the absence or presence of increasing concentrations of MW150, cells harvested after 1 h of stimulation for analysis of pMK2 and after 16 h for measurement of proinflammatory cytokine IL-1 β using kits from Meso Scale Discovery (MSD; Gaithersburg, Maryland).

Cell permeability and efflux pump susceptibility were determined by the standard Caco-2 two-way permeability analysis in the absence and presence of a known P-gp inhibitor, valsopodar, with monitoring of parent drug by HPLC/MS/MS. Similarly, the BCRP-MDCK cell system was used to determine MDCK cell permeability and potential substrate status for the efflux pump BCRP (breast cancer resistance protein) using two-way permeability measurement in the absence or presence of the known BCRP inhibitor, Ko143, with monitoring of parent drug by HPLC/MS/MS. The data shown are from experiments performed as a commercial service by Absorption Systems (Exton, PA).

The Ames test for genetic toxicology potential was done using a bacterial reverse mutation assay to evaluate the potential of MW150 to induce or reverse mutations with and without metabolic activation. Briefly, the ability to induce reverse mutations at loci of two strains of *Salmonella typhimurium* TA98 and TA100 was tested. MW150 was tested \pm metabolic activation at concentrations up to 5 μg /plate. The positive controls, 2-nitrofluorene for TA98 and sodium azide for TA100, and vehicle control were within expected ranges. Data presented are from commercial service assays performed by BioReliance, Inc. (Rockville, MD).

In Vivo Studies. The oral bioavailability of MW150 after intravenous (iv) and oral (po) administration in male Sprague–Dawley rats was done by Absorption Systems (Exton, PA). Briefly, MW150 (5 mg/kg) was administered to male rats (3 rats per treatment group; total $N = 6$) using MW01-2-151SRM as an internal standard. Animals were fasted for a minimum of 12 hours prior to administration until 4 h post dose. All animals showed normal activity during the study. Blood was collected via jugular vein cannulation at 5 min, 15 min, 30 min, 1 h, 3 h, and 6 h, and plasma generated and

stored at -60 to -80 $^{\circ}\text{C}$. Samples were analyzed by LS-MS/MS, and the pharmacokinetic parameters were estimated by a noncompartmental analysis. The brain-to-plasma ratio in male Sprague–Dawley rats was determined following a single oral administration of 5 mg/kg. Plasma and brain tissue samples were collected at 3 h post administration. Brain tissue was weighed, methanol/water (20:80) added to 4 mL/gram, and the sample homogenized (4 $^{\circ}\text{C}$) using a Virsonic 100 ultrasonic homogenizer and then frozen at -80 $^{\circ}\text{C}$. Homogenates were subjected to acetonitrile precipitation and supernatants analyzed by LC-MS/MS.

Behavior as pharmacodynamic test of in vivo efficacy was performed in two mouse models. The APP/PS1 transgenic mouse (Watterson et al.⁶) and the humanized knock-in mouse APP^{NLh/NLh} \times PS1^{P264L/P264L} and their WT controls were used as previously described.^{6,27} Repeat administration was done via intraperitoneal route. In compliance with animal use guidelines, the number of mice used was minimized by not administering MW150 to WT mice based on previous results in similar studies with the APP/PS1 KI mice. At the start, each experimental group contained mice of either sex, with the numbers of males and females in each group matched as closely as possible. Treatments and assays were done by personnel who were blind to genotype and drug treatment conditions.

■ ASSOCIATED CONTENT

📄 Supporting Information

Tables S1–S3; Figures S1–S3; additional methods, references, and spectra. This material is available free of charge via the Internet at <http://pubs.acs.org/>.

Accession Codes

The PDB code for human p38 α MAPK with bound MW150 is 4R3C.

■ AUTHOR INFORMATION

Corresponding Author

*Mailing address: Northwestern University, 303 E. Chicago Ave, Ward 8-196, Chicago, IL 60611. Telephone: 312-503-0657. E-mail: d.m.watterson@gmail.com.

Author Contributions

S. M. Roy designed and did organic syntheses, performed analytical chemistry analyses, evaluated bioanalytical results, and drafted the manuscript. V. L. Grum-Tokars performed crystallography and diffraction data experiments and modeling. J. P. Schavocky did enzyme assays and supervised pharmacology experiments. F. Saeed maintained the mouse colony and performed the treatment of the APP/PS1 Tg mice. A. Staniszewski performed the behavioral experiments on the APP/PS1 Tg mice. A. F. Teich performed histological analysis of the APP/PS1 Tg mice. O. Arancio designed efficacy studies, supervised experiments on the APP/PS1 Tg mice and drafted the manuscript. A. D. Bachstetter performed Abeta immunohistochemistry and the microglia cell culture experiments. S. J. Webster performed cognitive tests of the APP/PS1 KI mice. L. J. Van Eldik analyzed data, drafted the manuscript. G. Minasov did diffraction data analyses and modeling. W. F. Anderson supervised crystallography and diffraction data analyses. J. C. Pelletier designed and did organic syntheses. D. M. Watterson assisted with experimental design and performance, analyzed data, drafted the manuscript.

Funding

This research was supported in part by NIH Awards U01AG043415 (D.M.W. and O.A.) and R01AG031311 (D.M.W.), ADDF Award 261108 (D.M.W.), and a Thome Memorial Foundation Award (L.J.V.E.).

Notes

The authors declare no competing financial interest.

ACKNOWLEDGMENTS

We thank Ms. Danielle Gouling and Mr. Edgardo Dimayuga for excellent technical assistance, and N. VanTuyle and V. Shirinsky for project advice and assistance.

ABBREVIATIONS

A β , amyloid-beta; BCRP, breast cancer resistance protein; CD₃OD, deuterated methanol; CDCl₃, deuterated chloroform; CNS, central nervous system; CYPs, cytochrome P450 enzymes; DIPEA, diisopropylethylamine; DME, 1,2-dimethoxyethane; DMSO, dimethyl sulfoxide; EtOAc, ethyl acetate; HLM, human liver microsomes; HRMS, high resolution mass spectrometry; IL-1 β , Interleukin-1 beta; KI, knock-in; LC-HRMS, liquid chromatography-high resolution accurate mass spectrometry; LDA, lithium diisopropylamide; LPS, lipopolysaccharide; MAPK, mitogen activated protein kinase; MeOH, methanol; MW, molecular weight; MW150, MW01-18-150SRM; Na₂CO₃, sodium carbonate; P-gp, permeability glycoprotein; PD, pharmacodynamics; PK, pharmacokinetic; POBr₃, phosphorus oxybromide; POCl₃, phosphorus oxychloride; PSA, polar surface area; RLM, rat liver microsomes; THF, tetrahydrofuran; TMS, tetramethylsilane; WT, wild type

REFERENCES

- (1) U.S. Food and Drug Administration (2001) Novartis, NDA 021335.
- (2) Fabbro, D., Cowan-Jacob, S. W., Mobitz, H., and Martiny-Baron, G. (2012) Targeting cancer with small-molecular-weight kinase inhibitors. In *Methods in Molecular Biology* (Walker, J. M., Ed.), 1st ed., Vol. 795, pp 1–34, Humana Press, New York.
- (3) Rask-Andersen, M., Zhang, J., Fabbro, D., and Schiöth, H. B. (2014) Advances in kinase targeting: current clinical use and clinical trials. *Trends Pharmacol. Sci.* 35, 604–620.
- (4) O'Brien, Z., and Moghaddam, M. F. (2013) Small Molecule Kinase Inhibitors Approved by the FDA from 2000 to 2011: A Systematic review of preclinical ADME Data. *Expert Opin. Drug Metabol. Toxicol.* 9, 1597–1612.
- (5) Uitdehaag, J. C., Verkaar, F., Alwan, H., de Man, J., Buijsman, R. C., and Zaman, G. J. R. (2012) A guide to picking the most selective kinase inhibitor tool compounds for pharmacological validation of drug targets. *Br. J. Pharmacol.* 166, 858–876.
- (6) Watterson, D. M., Grum-Tokars, V. L., Roy, S. M., Schavocky, J. P., Bradaric, B. D., Bachstetter, A. D., Xing, B., Dimayuga, E., Saeed, F., Zhang, H., Staniszewski, A., Pelletier, J. C., Minasov, G., Anderson, W. F., Arancio, O., and Van Eldik, L. J. (2013) Development of novel in vivo chemical probes to address CNS protein kinase involvement in synaptic dysfunction. *PLoS One* 8, e66226.
- (7) Pardridge, W. M. (2005) Blood-brain barrier: Bottleneck in brain drug development. *NeuroRx* 2, 3–14.
- (8) Munoz, L., and Ammit, A. J. (2010) Targeting p38 MAPK pathway for the treatment of Alzheimer's disease. *Neuropharmacology* 58, 561–568.
- (9) Bachstetter, A. D., Watterson, D. M., and Van Eldik, L. J. (2014) Target engagement analysis and link to pharmacodynamics endpoint for a novel class of CNS-penetrant and efficacious p38 α MAPK inhibitors. *J. Neuroimmune Pharmacol.* 9, 454–460.
- (10) Chavkin, C., Schattauer, S. S., and Levin, J. R. (2014) Arrestin-Mediated Activation of p38 MAPK: molecular mechanism and behavioral consequences. In *Handbook of Experimental Pharmacology* (Berlin, W. R., Ed), 1st ed, Vol. 219, pp 281–292, Springer Press, New York.
- (11) Berg, J. M., Rogers, M. E., and Lyster, P. M. (2010) Systems biology and pharmacology. *Clin. Pharmacol. Ther.* 88, 17–19.
- (12) Munoz, L., Ralay Ranaivo, H., Roy, S. M., Hu, W., Craft, J. M., McNamara, L. K., Wing Chico, L., Van Eldik, L. J., and Watterson, D. M. (2007) A novel p38 α MAPK inhibitor suppresses brain proinflammatory cytokine up-regulation and attenuates synaptic dysfunction and behavioral deficits in an Alzheimer's disease mouse model. *J. Neuroinflammation* 4, 21.
- (13) Tong, L., Prieto, G. A., Kramar, E. A., Smith, E. D., Cribbs, D. H., Lynch, G., and Cotman, C. W. (2012) Brain-derived neurotrophic factor-dependent synaptic plasticity is suppressed by interleukin-1 β via p38 mitogen-activated protein kinase. *J. Neurosci.* 32, 17714–17724.
- (14) Duma, R. S., and Aghajanian, G. K. (2012) Synaptic dysfunction in depression: potential therapeutic targets. *Science* 338, 68–72.
- (15) Picconi, B., Piccoli, G., and Calabresi, P. (2012) Synaptic dysfunction in Parkinson's disease. *Adv. Exp. Med. Biol.* 970, 553–572.
- (16) Correa, S. A., and Eales, K. L. (2012) The role of p38 MAPK and its substrates in neuronal plasticity and neurodegenerative disease. *J. Signal Transduction* 2012, 649079.
- (17) Zhu, C. B., Steiner, J. A., Munn, J. L., Daws, L. C., Hewlett, W. A., and Blakely, R. D. (2007) Rapid stimulation of presynaptic serotonin transport by A (3) adenosine receptors. *J. Pharmacol. Exp. Ther.* 322, 332–340.
- (18) Samuvel, D. J., Jayanthi, L. D., Bhat, N. R., and Ramamoorthy, S. (2005) A role for p38 mitogen-activated protein kinase in the regulation of the serotonin transporter: Evidence for distinct cellular mechanisms involved in transporter surface expression. *J. Neurosci.* 25, 29–41.
- (19) Bruchas, M. R., Schindler, A. G., Shankar, H., Messinger, D. I., Miyatake, M., Land, B. B., Lemos, J. C., Hagan, C. E., Neumaier, J. F., Quintana, A., Palmiter, R. D., and Chavkin, C. (2011) Selective p38 α MAPK Deletion in Serotonergic Neurons Produces Stress Resilience in Models of Depression and Addiction. *Neuron* 71, 498–511.
- (20) Zhan, L., Xie, Q., and Tibbetts, R. S. (2015) Opposing roles of p38 and JNK in a *Drosophila* model of TDP-43 proteinopathy reveal oxidative stress and innate immunity as pathogenic components of neurodegeneration. *Hum. Mol. Genet.* 24, 757–772.
- (21) Zhu, C. B., Hewlett, W. A., Feoktistov, I., Biaggioni, I., and Blakely, R. D. (2004) Adenosine receptor, protein kinase G, and p38 mitogen-activated protein kinase-dependent up-regulation of serotonin transporters involves both transporter trafficking and activation. *Mol. Pharmacol.* 65, 1462–1474.
- (22) Zhu, C. B., Carneiro, A. M., Dostmann, W. R., Hewlett, W. A., and Blakely, R. D. (2005) p38 MAPK activation elevates serotonin transport activity via a trafficking-independent, protein phosphatase 2A-dependent process. *J. Biol. Chem.* 280, 15649–15658.
- (23) Morfini, G. A., Bosco, D. A., Brown, H., Gatto, R., Kaminska, A., Song, Y., Molla, L., Baker, L., Marangoni, M. N., Berth, S., Tavassoli, E., Bagnato, C., Tiwari, A., Hayward, L. J., Pigino, G. F., Watterson, D. M., Huang, C.-F., Banker, G., Brown, R. H., Jr., and Brady, S. T. (2013) Inhibition of Fast Axonal Transport by Oathogenic SOD1 involves Activation of p38 MAP Kinase. *PLoS One* 8, e65235.
- (24) Hu, W., Ralay Ranaivo, H., Roy, S. M., Behanna, H. A., Wing, L. K., Munoz, L., Guo, L., Van Eldik, L. J., and Watterson, D. M. (2007) Development of a novel therapeutic suppressor of brain proinflammatory cytokine up-regulation that attenuates synaptic dysfunction and behavioral deficits. *Bioorg. Med. Chem. Lett.* 17, 414–418.
- (25) Chico, L. K., Van Eldik, L. J., and Watterson, D. M. (2009) Targeting protein kinases in central nervous system disorders. *Nat. Rev. Drug Discovery* 8, 892–909.
- (26) Chico, L. K., Behanna, H. A., Hu, W., Zhong, G., Roy, S. M., and Watterson, D. M. (2009) Molecular properties and CYP2D6 substrates: central nervous system therapeutics case study and pattern analysis of a substrate database. *Drug Metab. Dispos.* 37, 2204–2211.
- (27) Bachstetter, A. D., Norris, C. M., Sompol, P., Wilcock, D. M., Gouling, D., Neltner, J. H., St. Clair, D., Watterson, D. M., and Van Eldik, L. J. (2012) Early stage drug treatment that normalizes proinflammatory cytokine production attenuates synaptic dysfunction in a mouse model that exhibits age-dependent progression of Alzheimer's disease-related pathology. *J. Neurosci.* 32, 10201–10210.

(28) U.S. Food and Drug Administration (2008) *Guidance for industry Q3A Impurities in New Drug substances*, U.S. Department of Health and Human Services Food and Drug Administration, Center for Drug Evaluation and Research (CDER) and Center for Biologics Evaluation and Research (CBER), www.fda.gov/downloads/drugs/guidancecomplianceregulatoryinformation/guidances/ucm073385.pdf.

(29) Reynolds, C. H. (2014) Protein–Ligand Cocrystal Structures: We Can Do Better. *ACS Med. Chem. Lett.* 5, 727–729.

(30) U.S. Food and Drug Administration (2001) *Guidance for Industry S7A Safety Pharmacology Studies for human Pharmaceuticals*. U.S. Department of Health and Human Services Food and Drug Administration, Center for Drug Evaluation and Research (CDER) and Center for Biologics Evaluation and Research (CBER), www.fda.gov/downloads/drugs/guidancecomplianceregulatoryinformation/guidances/ucm074959.pdf.

(31) Wilcock, D. M., and Colton, C. A. (2009) Immunotherapy, vascular pathology and microhemorrhages in transgenic mice. *CNS Neurol. Disord.: Drug Targets* 8, 50–64.

(32) Li, L., Li, G., Yu, C., and Li, Y. (2013) A meta-analysis of the role of p38 mitogen-activated protein kinase inhibitors in patients with active rheumatoid arthritis. *Clin. Rheumatol.* 32, 1697–1702.

(33) Newby, L. K., Marber, M. S., Melloni, C., Sarov-Blat, L., Aberle, L. H., Aylward, P. E., Cai, G., de Winter, R. J., Hamm, C. W., Heitner, J. F., Kim, R., Lerman, A., Patel, M. R., Tanguay, J. F., Lepore, J. J., Al-Khalidi, H. R., Sprecher, D. L., Granger, C. B., et al. (2014) Losmapimod, a novel p38 mitogen-activated protein kinase inhibitors, in non-ST-segment elevation myocardial infarction: a randomized phase 2 trial. *J. Lancet* 384, 1187–1195.

(34) Avdeef, A., Comer, J. E. A., and Thomson, S. J. (1993) pH-metric logP. 3. Glass electrode calibration in methanol-water, applied to pK_a determination of water-insoluble substances. *Anal. Chem.* 65, 42–49.